

Protection of a Qubit via Subradiance: A Josephson Quantum Filter

Kazuki Koshino^{1,*}, Shingo Kono^{1,2}, and Yasunobu Nakamura^{2,3}

¹College of Liberal Arts and Sciences, Tokyo Medical and Dental University (TMDU), Ichikawa, Chiba 272-0827, Japan

²RIKEN Center for Emergent Matter Science (CEMS), 2-1 Hirosawa, Wako, Saitama 351-0198, Japan

³Research Center for Advanced Science and Technology (RCAST), The University of Tokyo, Meguro-ku, Tokyo 153-8904, Japan



(Received 15 September 2019; revised manuscript received 9 December 2019; published 27 January 2020)

The coupling between a superconducting qubit and a control line inevitably results in radiative decay of the qubit into the line. We propose a Josephson quantum filter (JQF), which protects the data qubit (DQ) from radiative decay through the control line without reducing the gate speed on the DQ. The JQF consists of a qubit strongly coupled to the control line of the DQ and its working principle is a subradiance effect that is characteristic of waveguide quantum electrodynamics setups. The JQF is a passive circuit element and is therefore suitable for integration in a scalable superconducting qubit system.

DOI: 10.1103/PhysRevApplied.13.014051

I. INTRODUCTION

The superconducting qubit system has high designability and *in situ* tunability of the system parameters and is therefore suitable for realization of scalable quantum computation. Supported by recent progress in integrating superconducting qubits, quantum computers including several tens of qubits are currently available [1–6]. In order to perform quantum-computational tasks involving many qubits, we need to apply fast gate operations on the qubits, while keeping the long coherence times of the qubits. These requirements are, however, usually conflicting. For gate operations on a superconducting qubit, we couple the qubit to a control line through which microwave gate pulses are applied. A strong coupling between the qubit and the control line is advantageous for the gate speed but is disadvantageous for the qubit lifetime due to radiative decay through the line. When the radiative decay rate of the qubit is γ , the Rabi frequency induced by a drive field applied through the line scales as $\gamma^{1/2}$ for a fixed drive power. Therefore, the gate speed and the qubit lifetime are proportional to $\gamma^{1/2}$ and γ^{-1} , respectively. A usual strategy to simultaneously realize a long qubit lifetime and fast gate operations is to make γ small in order to enhance the qubit lifetime and to apply short and intense pulses to reduce the gate time. For example, we can halve the gate time by doubling the amplitude of the control pulse. This results, however, in doubling of the average photon number per pulse and, consequently, more heating of the surrounding components, such as the attenuators and filters passing the

pulse. Intense control pulses may also induce unwanted crosstalk with neighboring qubits and resonators.

In the dispersive readout of qubits [7–9], a similar trade-off exists between the measurement speed and the qubit lifetime. In this scheme, we couple the qubit dispersively to a resonator and then to a readout line, through which readout microwave pulses are applied. A strong coupling between the resonator and the readout line enables fast measurements but shortens the qubit lifetime due to resonator-mediated radiative decay (the Purcell effect) [10]. Here, the readout frequency is essentially that of the resonator, whereas the frequency of an emitted photon is that of the qubit. Using this frequency difference, we can resolve the trade-off by incorporating a frequency filter (a Purcell filter) in the readout line [9,11–14]. However, such frequency filtering is unsuitable for the suppression of decay into the control line, since the control pulses should be resonant to the qubit and therefore have the same frequency as the leaking photon. If we incorporate a conventional Purcell filter in the control line, the filter attenuates the control pulse and reduces the gate speed, although it will enhance the qubit lifetime.

In this study, we propose a filter that prohibits radiative decay of the qubit into the control line while not affecting the control speed. Figure 1 is a schematic of the considered setup: a data qubit (DQ) to be controlled is coupled to one end of a semi-infinite control line, and a filter qubit, which is referred to as a Josephson quantum filter (JQF), is placed at a distance of the order of the resonance wavelength of the DQ. In such waveguide-QED setups, it is known that a qubit functions as a nonlinear mirror, which completely reflects a weak field due to destructive interference and transmits a stronger field due to absorption saturation

*kazuki.koshino@osamember.org

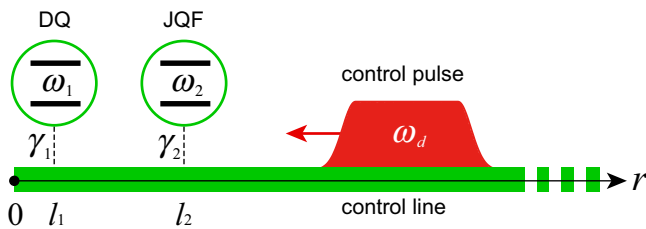


FIG. 1. A schematic of the setup. The DQ and the JQF are directly coupled to a semi-infinite waveguide, through which control pulses for the DQ are applied. Unless otherwise specified, the following parameter values are assumed: $\omega_1/2\pi = \omega_2/2\pi = 5$ GHz (resonance wavelength $\lambda_q = 20$ mm, for the microwave velocity $v = 10^8$ m/s), $l_1 = 0$ mm, $l_2 = \lambda_q/2 = 10$ mm, $\gamma_1/2\pi = 2$ kHz, and $\gamma_2/2\pi = 100$ MHz.

[15–19]. In radiative decay of a DQ, where only a single photon is concerned, the JQF works as a mirror that prohibits radiative decay of the DQ. On the other hand, when we perform gate operations on the DQ by applying strong control pulses, the JQF transmits the pulses and does not reduce the gate speed. Thus, the working principle of the JQF is in its nonlinear microwave response. This point is in clear contrast with a conventional Purcell filter, the microwave response of which is completely linear. Since the JQF is a passive circuit element that is free from the imposition of active control, the JQF is ready to be incorporated in complicated circuits involving many qubits. Together with established schemes such as Purcell filters [11–14] and tunable qubit-waveguide couplers [20–22], the JQF would be highly useful for constructing a network of long-lived qubits and yet allowing fast control and measurements.

The rest of this paper is organized as follows. In Sec. II, we theoretically describe the considered setup. We present the Hamiltonian of the overall system composed of the DQ, the JQF, and a semi-infinite control line, and derive their Heisenberg equations. In Sec. III, assuming the absence of the JQF, we review the trade-off between the gate speed and the lifetime of the DQ. In Sec. IV, we analyze the radiative decay of the initially excited DQ. We derive an analytical formula for the radiative decay rate of the DQ and clarify the condition that the JQF protects the DQ from radiative decay. In Sec. V, we numerically examine the microwave response of the DQ and the JQF to confirm the following: the JQF does not affect the dynamics of the DQ induced by the control field and therefore does not reduce the gate speed. At the same time, the JQF prohibits radiative decay of the DQ while the control field is off. Section VI is devoted to the summary.

II. FORMULATION

A. Hamiltonian

The physical setup considered in this study is schematically illustrated in Fig. 1. In order to apply control

microwave pulses to the DQ (qubit 1), we attach a semi-infinite waveguide to the DQ. In front of the DQ, we attach the JQF (qubit 2), which is also a qubit with the same frequency as the DQ. The semi-infinite waveguide extends in the $r > 0$ region. Its eigenmodes are standing waves, which are continuously labeled by a wave number $k(> 0)$. Assuming an open boundary condition at the termination point ($r = 0$), the mode function $f_k(r)$ is given by

$$f_k(r) = \sqrt{\frac{2}{\pi}} \cos kr. \quad (1)$$

We denote the annihilation operator for this mode by \hat{b}_k . The mode functions are normalized as $\int_0^\infty dr f_{k'}^*(r)f_k(r) = \delta(k - k')$.

Both qubits can be regarded as two-level systems. We denote the lowering operator of qubit m ($m = 1, 2$) by $\hat{\sigma}_m$, the transition frequency by ω_m , the coupling position to the waveguide by l_m , and the coupling strength by γ_m . Note that γ_m represents the radiative decay rate of qubit m , assuming that the qubit is coupled to an *infinite* waveguide.

Setting $\hbar = v = 1$, where v is the microwave velocity in the waveguide, the Hamiltonian of the overall system composed of the DQ, the JQF, and the semi-infinite waveguide is given by

$$\begin{aligned} \hat{H} = & \sum_m \omega_m \hat{\sigma}_m^\dagger \hat{\sigma}_m \\ & + \int_0^\infty dk \left[k \hat{b}_k^\dagger \hat{b}_k + \sum_m g_{mk} (\hat{\sigma}_m^\dagger \hat{b}_k + \hat{b}_k^\dagger \hat{\sigma}_m) \right], \end{aligned} \quad (2)$$

where the coupling constant g_{mk} is given by

$$g_{mk} = \sqrt{\frac{\gamma_m}{2}} f_k(l_m) = \sqrt{\frac{\gamma_m}{\pi}} \cos(kl_m). \quad (3)$$

In this study, we aim to protect the DQ from radiative decay using the JQF. For this purpose, the system parameters are chosen as follows. (i) The two qubits are nearly resonant, i.e., $\omega_1 \approx \omega_2 \approx \omega_q$. (ii) The positions l_1 and l_2 of the qubits are of the order of their resonance wavelength, $\lambda_q = 2\pi v/\omega_q$. The DQ is closer to the end of the waveguide than the JQF, i.e., $0 \leq l_1 \leq l_2$. (iii) The coupling between the JQF and the waveguide is much stronger than that of the DQ, i.e., $\gamma_1 \ll \gamma_2$. Unless otherwise specified, we employ the parameter values listed in the caption of Fig. 1.

For a semi-infinite waveguide, the wave number k of the waveguide mode is restricted to be positive. However, we formally extend the lower limit of k to $-\infty$ [23], and introduce the real-space representation \tilde{b}_r of the field operator

by

$$\tilde{b}_r = \frac{1}{\sqrt{2\pi}} \int_{-\infty}^{\infty} dk e^{ikr} \hat{b}_k. \quad (4)$$

The space variable r runs over $-\infty < r < \infty$: the negative (positive) region represents the incoming (outgoing) field. The introduction of the real-space representation is validated by a rigorous “modes of the universe” approach [24].

B. Heisenberg equations

The Heisenberg equation for \hat{b}_k is given by $(d/dt)\hat{b}_k = -ik\hat{b}_k - i \sum_m g_{mk} \hat{\sigma}_m$. This is formally solved as

$$\hat{b}_k(t) = \hat{b}_k(0)e^{-ikt} - i \sum_m g_{mk} \int_0^t dt' \hat{\sigma}_m(t') e^{ik(t'-t)}. \quad (5)$$

Switching to the real-space representation with Eq. (4), we have

$$\begin{aligned} \tilde{b}_r(t) = & \tilde{b}_{r-t}(0) - i \sum_m \sqrt{\frac{\gamma_m}{2}} [\Theta_{r \in (-l_m, t-l_m)} \hat{\sigma}_m(t-r-l_m) \\ & + \Theta_{r \in (l_m, t+l_m)} \hat{\sigma}_m(t-r+l_m)], \end{aligned} \quad (6)$$

where Θ is a product of the step functions, $\Theta_{r \in (a,b)} = \theta(r-a)\theta(b-r)$. This equation plays the role of the input-output relation in quantum optics [25,26].

The Heisenberg equation for a system operator \hat{o} (composed of $\hat{\sigma}_1$, $\hat{\sigma}_2$, and their conjugates) is written, from Eqs. (2) and (4), as

$$\begin{aligned} \frac{d}{dt} \hat{o} = & i[\hat{H}_s, \hat{o}] + i \sum_m \sqrt{\frac{\gamma_m}{2}} \{ [\hat{\sigma}_m^\dagger, \hat{o}] \{ \tilde{b}_{l_m}(t) + \tilde{b}_{-l_m}(t) \} \\ & + \{ \tilde{b}_{l_m}^\dagger(t) + \tilde{b}_{-l_m}^\dagger(t) \} [\hat{\sigma}_m, \hat{o}] \}, \end{aligned} \quad (7)$$

where $\hat{H}_s = \sum_m \omega_m \hat{\sigma}_m^\dagger \hat{\sigma}_m$. From Eq. (6), we obtain the following equality:

$$\begin{aligned} \tilde{b}_{l_m}(t) + \tilde{b}_{-l_m}(t) = & \tilde{b}_{l_m-t}(0) + \tilde{b}_{-l_m-t}(0) \\ & - i \sum_n \sqrt{\frac{\gamma_n}{2}} [\hat{\sigma}_n(t-l_m-l_n) + \hat{\sigma}_n(t-|l_m-l_n|)]. \end{aligned} \quad (8)$$

From Eqs. (7) and (8), we have

$$\begin{aligned} \frac{d}{dt} \hat{o} = & i[\hat{H}_s, \hat{o}] + i \sum_m \{ [\hat{\sigma}_m^\dagger, \hat{o}] \hat{N}_m(t) + \hat{N}_m^\dagger(t) [\hat{\sigma}_m, \hat{o}] \} \\ & + \sum_{m,n} \frac{\sqrt{\gamma_m \gamma_n}}{2} [\hat{\sigma}_m^\dagger, \hat{o}] \{ \hat{\sigma}_n(t-l_m-l_n) \} \end{aligned}$$

$$\begin{aligned} & + \hat{\sigma}_n(t-|l_m-l_n|) \} - \sum_{m,n} \frac{\sqrt{\gamma_m \gamma_n}}{2} \{ \hat{\sigma}_n^\dagger(t-l_m-l_n) \\ & + \hat{\sigma}_n^\dagger(t-|l_m-l_n|) \} [\hat{\sigma}_m, \hat{o}]. \end{aligned} \quad (9)$$

Note that the explicit time dependence is omitted for operators at time t and that the operators with a negative time variable should be replaced with zero. The noise operator $\hat{N}_m(t)$ for qubit m is defined by

$$\hat{N}_m(t) = \sqrt{\frac{\gamma_m}{2}} [\tilde{b}_{l_m-t}(0) + \tilde{b}_{-l_m-t}(0)]. \quad (10)$$

C. Free-evolution approximation

The Heisenberg equation (9), which is driven from the Hamiltonian of Eq. (2), contains qubit operators with retarded times. However, considering that the qubit decay during such retardation is negligibly small ($\gamma_m l_m/v \ll 1$), we can employ the free-evolution approximation [27,28], $\hat{\sigma}_m(t-\Delta t) \approx e^{i\omega_q \Delta t} \hat{\sigma}_m(t)$. The validity of this approximation is confirmed in Appendix A. Then, Eq. (9) is recast into the following simpler form:

$$\begin{aligned} \frac{d}{dt} \hat{o} = & i[\hat{H}_s, \hat{o}] + i \sum_m \{ [\hat{\sigma}_m^\dagger, \hat{o}] \hat{N}_m(t) + \hat{N}_m^\dagger(t) [\hat{\sigma}_m, \hat{o}] \} \\ & + \sum_{m,n} (\xi_{mn} [\hat{\sigma}_m^\dagger, \hat{o}] \hat{\sigma}_n - \xi_{mn}^* \hat{\sigma}_n^\dagger [\hat{\sigma}_m, \hat{o}]), \end{aligned} \quad (11)$$

$$\xi_{mn} = \frac{\sqrt{\gamma_m \gamma_n}}{2} (e^{i\omega_q(l_m+l_n)} + e^{i\omega_q(|l_m-l_n|)}). \quad (12)$$

Although direct interaction between the DQ and the JQF is absent in the Hamiltonian of Eq. (2), virtual-waveguide photons mediate an effective interaction between them, which appears as $\xi_{12} = \xi_{21} = \sqrt{\gamma_1 \gamma_2} \cos(\omega_q l_1) e^{i\omega_q l_2}$. Note that the roles of the DQ and the JQF are asymmetric in this interaction due to the semi-in infiniteness of the control line.

Since the detuning of the control pulse from the qubit resonance, $\omega_d - \omega_q$, is small enough to satisfy $(\omega_d - \omega_q)l_m/v \ll 1$ in the considered setup, we can make the following approximation: $\tilde{b}_{\Delta r-t}(0) \approx e^{i\omega_q \Delta r} \tilde{b}_{-t}(0)$. We then have

$$\hat{N}_m(t) = \sqrt{2\gamma_m} \cos(\omega_q l_m) \tilde{b}_{-t}(0). \quad (13)$$

For future reference, setting $\hat{o} = \hat{\sigma}_1$, we have

$$\begin{aligned} \frac{d}{dt} \hat{\sigma}_1 = & (-i\omega_q - \xi_{11}) \hat{\sigma}_1 - \xi_{12} (1 - 2\hat{\sigma}_1^\dagger \hat{\sigma}_1) \hat{\sigma}_2 \\ & - i(1 - 2\hat{\sigma}_1^\dagger \hat{\sigma}_1) \hat{N}_1(t). \end{aligned} \quad (14)$$

D. Effective interaction and cooperative dissipator

In the preceding theoretical works dealing with the qubit system coupled to an infinite waveguide [29–32], the

photon-mediated qubit-qubit interaction is treated by the effective-dipole exchange interaction \hat{H}_e and the cooperative dissipator \hat{S} . Here, we rewrite Eqs. (11) and (12) in this form for reference. Dividing ξ_{mn} into real and imaginary parts, we have

$$\begin{aligned} \frac{d}{dt}\hat{o} &= i[\hat{H}_s + \hat{H}_e, \hat{o}] + \frac{[\hat{S}^\dagger, \hat{o}]\hat{S} + \hat{S}^\dagger[\hat{o}, \hat{S}]}{2} \\ &\quad + i\left\{\hat{b}_{in}^\dagger(t)[\hat{S}, \hat{o}] + [\hat{S}^\dagger, \hat{o}]\hat{b}_{in}(t)\right\}, \end{aligned} \quad (15)$$

$$\hat{H}_e = \sum_{m,n} J_{mn} \hat{\sigma}_m^\dagger \hat{\sigma}_n, \quad (16)$$

$$\hat{S} = \sum_m \sqrt{2\gamma_m} \cos(\omega_q l_m) \hat{\sigma}_m, \quad (17)$$

$$J_{mn} = \sqrt{\gamma_m \gamma_n} \cos[\omega_q \min(l_m, l_n)] \sin[\omega_q \max(l_m, l_n)], \quad (18)$$

where $\hat{b}_{in}(t) = \tilde{b}_{-t}(0)$. Three comments are in order regarding the above equations. (i) The cooperative dissipator \hat{S} and the effective interaction \hat{H}_e result from the real and imaginary parts of ξ_{mn} , respectively. (ii) In the case of an infinite waveguide, two kinds of cooperative dissipators appear, corresponding to the positively and negatively propagating modes. Here, the cooperative dissipator \hat{S} is unique and the cosine function appearing in \hat{S} results from the standing-wave mode function [Eq. (1)]. (iii) In the case of an infinite waveguide, the coefficient J_{mn} of the effective interaction depends only on the mutual distance between the qubits, $|l_m - l_n|$. Here, J_{mn} has a more complicated form due to the semi-infiniteness of the waveguide.

III. TRADE-OFF BETWEEN QUBIT LIFETIME AND GATE SPEED

In this section, we observe the trade-off between the lifetime of the DQ and the gate speed, assuming the absence of the JQF ($\gamma_2 = 0$). The Heisenberg equation (14) for $\hat{\sigma}_1$ is then rewritten as

$$\frac{d}{dt}\hat{\sigma}_1 = (-i\bar{\omega}_q - \eta^2/2)\hat{\sigma}_1 - i\eta(1 - 2\hat{\sigma}_1^\dagger\hat{\sigma}_1)\tilde{b}_{-t}(0), \quad (19)$$

where $\bar{\omega}_q = \omega_q + (\gamma_1/2) \sin(2\omega_q l_1)$ is the renormalized qubit frequency including the Lamb shift. A real constant $\eta = \sqrt{2\gamma_1} \cos(\omega_q l_1)$ has two roles that originate in the fluctuation-dissipation theorem: the radiative decay rate of the qubit and the coupling between the qubit and the applied field.

In the absence of the input field, the qubit excitation probability decays as $d/dt\langle\hat{\sigma}_1^\dagger\hat{\sigma}_1\rangle = -\eta^2\langle\hat{\sigma}_1^\dagger\hat{\sigma}_1\rangle$. Therefore, the qubit radiative lifetime T_r is given by

$$T_r = \frac{1}{\eta^2}. \quad (20)$$

Note that, when coupled to a semi-infinite waveguide, the radiative lifetime depends on the qubit position l_1 due to the broken translation symmetry. On the other hand, when we apply a resonant control field $E_{in}(t) = E_d e^{-i\bar{\omega}_q t}$ through the waveguide, the qubit excitation probability evolves as $d^2/dt^2\langle\hat{\sigma}_1^\dagger\hat{\sigma}_1\rangle = 2\eta^2|E_d|^2(1 - 2\langle\hat{\sigma}_1^\dagger\hat{\sigma}_1\rangle)$ and exhibits the Rabi oscillation with the Rabi frequency of $\Omega_R = 2\eta|E_d|$. Therefore, the gate speed T_g^{-1} for a π pulse is given by

$$T_g^{-1} = \frac{2\eta|E_d|}{\pi}. \quad (21)$$

Thus, there exists a trade-off between the qubit radiative lifetime and the gate speed. The overall lifetime T_1 of the qubit is always shorter than the radiative lifetime T_r due to other relaxation channels. Therefore, from Eqs. (20) and (21), we have the following inequality:

$$T_1 \left(\frac{1}{T_g} \right)^2 \leq \frac{4|E_d|^2}{\pi^2}, \quad (22)$$

where $|E_d|^2$ in the right-hand side represents the photon rate of the applied field. This is limited, besides the practical reasons, by the finite anharmonicity of the qubit, which is particularly small for the transmon-type qubits.

IV. RADIATIVE DECAY

In this section, we analytically investigate the radiative decay of the DQ in the presence of the JQF and clarify the optimal condition for the JQF. As the initial state, we consider a state in which only the DQ is excited. The state vector is written as

$$|\psi(0)\rangle = \hat{\sigma}_1^\dagger |v\rangle, \quad (23)$$

where $|v\rangle$ represents the vacuum state of the whole setup. Since the Hamiltonian of Eq. (2) conserves the total excitation number, the state vector at time t , $|\psi(t)\rangle = e^{-i\hat{H}t}|\psi(0)\rangle$, is written as follows:

$$|\psi(t)\rangle = \sum_{m=1,2} \alpha_m(t) \hat{\sigma}_m^\dagger |v\rangle + \int dr f(r, t) \tilde{b}_r^\dagger |v\rangle, \quad (24)$$

where the coefficients $\alpha_m(t)$ and the wave packet of the emitted photon $f(r, t)$ satisfy the normalization condition of $\sum_m |\alpha_m(t)|^2 + \int_0^t dr |f(r, t)|^2 = 1$. Using the fact that $\hat{H}|v\rangle = 0$, we have $\alpha_m(t) = \langle v|\hat{\sigma}_m|\psi(t)\rangle = \langle v|\hat{\sigma}_m(t)\hat{\sigma}_1^\dagger(0)|v\rangle$. From Eq. (14) and its counterpart for

$\hat{\sigma}_2(t)$, the equations of motion for $\alpha_m(t)$ are given by

$$\frac{d\alpha_1}{dt} = -(i\omega_q + \xi_{11})\alpha_1 - \xi_{12}\alpha_2, \quad (25)$$

$$\frac{d\alpha_2}{dt} = -\xi_{21}\alpha_1 - (i\omega_q + \xi_{22})\alpha_2, \quad (26)$$

with the initial conditions of $\alpha_1(0) = 1$ and $\alpha_2(0) = 0$. In deriving the above equations, we use $\hat{N}_m(t)|\psi(0)\rangle = 0$ and $\hat{\sigma}_1(t)\hat{\sigma}_2(t)\hat{\sigma}_m^\dagger(0)|v\rangle = 0$. For reference, the wave packet of the emitted photon is given by $f(r, t) = -i\sqrt{2\gamma_1} \cos(\omega_q l_1)\alpha_1(t-r) - i\sqrt{2\gamma_2} \cos(\omega_q l_2)\alpha_2(t-r)$ for $0 \leq r \leq t$, and $f(r, t) = 0$ otherwise.

A. Decay rate of the DQ

In the absence of the photon-mediated interaction between qubits, the complex frequency of qubit m is given by $\tilde{\omega}_m = \omega_q - i\xi_{mm}$ and the radiative decay rate is given by $-2\text{Im}(\tilde{\omega}_m) = 2\gamma_m \cos^2(\omega_q l_m)$. Therefore, except for the special case of $l_2 \approx (1 + 2n/4)\lambda_q$ ($n = 0, 1, \dots$), where $\lambda_q = 2\pi\nu/\omega_q$ is the resonance wavelength of the qubits, the JQF decays much faster than the DQ. Then, by switching to the frame rotating at ω_q and applying the adiabatic approximation, Eq. (26) reduces to $\alpha_2(t) \approx -(\xi_{21}/\xi_{22})\alpha_1(t)$. Substituting this into Eq. (25), we confirm that the complex frequency $\tilde{\omega}'_1$ of the DQ reduces to a real quantity:

$$\tilde{\omega}'_1 = \omega_q - \gamma_1 \frac{\cos(\omega_q l_1) \sin[\omega_q(l_2 - l_1)]}{\cos(\omega_q l_2)}. \quad (27)$$

This implies that, owing to the JQF, the DQ acquires an infinite radiative lifetime regardless of its position l_1 ($< l_2$).

For comparison, we consider the case of $l_1 > l_2$. The renormalized complex frequency of the DQ is then given by

$$\tilde{\omega}''_1 = \omega_q - \gamma_1 e^{i\omega_q(l_1 - l_2)} \sin[\omega_q(l_1 - l_2)], \quad (28)$$

the imaginary part of which vanishes only when $\sin[\omega_q(l_1 - l_2)] = 0$. Therefore, in contrast with the case

of $l_1 < l_2$, the radiative decay of the DQ is prohibited only when the DQ is located exactly at $l_1 = l_2 + n\lambda_q/2$ ($n = 0, 1, \dots$).

The effect of the intrinsic decay of the JQF other than the radiative decay into the line, which is assumed to be absent throughout this paper, is discussed in Appendix B. It is revealed there that the radiative decay rate of the DQ is suppressed by a factor of γ_{12}/γ_2 , where γ_{12} (γ_2) is the intrinsic (radiative) decay rate of the JQF. Therefore, the suppression becomes imperfect when the JQF has a finite intrinsic decay rate but is still substantial if $\gamma_{12} \ll \gamma_2$.

B. Time evolution

The solutions of Eqs. (25) and (26) are given by

$$\alpha_1(t) = \left(\frac{\mu_2 + \xi_{11}}{\mu_2 - \mu_1} e^{\mu_1 t} + \frac{\mu_1 + \xi_{11}}{\mu_1 - \mu_2} e^{\mu_2 t} \right) e^{-i\omega_q t}, \quad (29)$$

$$\alpha_2(t) = \frac{\xi_{21}}{\mu_2 - \mu_1} (e^{\mu_1 t} - e^{\mu_2 t}) e^{-i\omega_q t}, \quad (30)$$

where μ_1 and μ_2 are the two solutions of the following quadratic equation for z :

$$(z + \xi_{11})(z + \xi_{22}) - \xi_{12}\xi_{21} = 0. \quad (31)$$

The survival probability of the DQ is given by $P_1(t) = |\alpha_1(t)|^2$. In Fig. 2, fixing the position of the DQ at $l_1 = 0$, the time evolution of $P_1(t)$ is shown for several values of l_2 . As expected, we observe that the decay of the DQ is suppressed, except when $l_2 \approx (1 + 2n)\lambda_q/4$. The optimal position of the JQF is $l_2 = n\lambda_q/2$. Equations (29) and (30) then reduce to the following forms:

$$\alpha_1(t) = \left(\frac{\gamma_2}{\gamma_1 + \gamma_2} + \frac{\gamma_1}{\gamma_1 + \gamma_2} e^{-(\gamma_1 + \gamma_2)t} \right) e^{-i\omega_q t}, \quad (32)$$

$$\alpha_2(t) = (-)^{n+1} \frac{\sqrt{\gamma_1 \gamma_2}}{\gamma_1 + \gamma_2} [1 - e^{-(\gamma_1 + \gamma_2)t}] e^{-i\omega_q t}. \quad (33)$$

In the limit as $t \rightarrow \infty$, $P_1(t) = \gamma_2^2/(\gamma_1 + \gamma_2)^2 \approx 1 - 2\gamma_1/\gamma_2$. Therefore, the radiative decay of the DQ is mostly prohibited when $\gamma_2 \gg \gamma_1$.

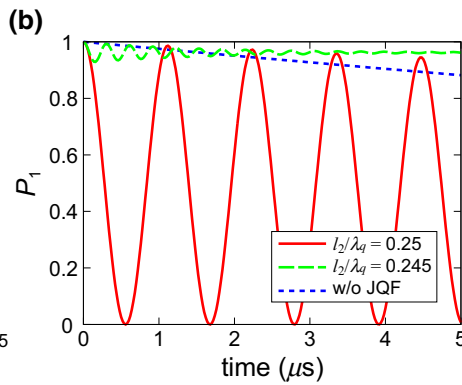
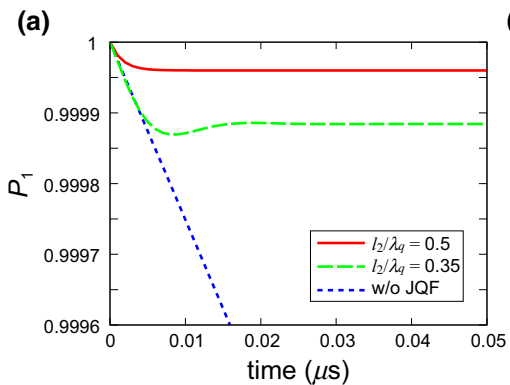


FIG. 2. The survival probability of the DQ, $P_1(t) = |\alpha_1(t)|^2$. The parameter values are described in the caption of Fig. 1, except that the JQF position l_2 is varied. (a) Results for $l_2/\lambda_q = 0.5$ (red solid line) and 0.35 (green dashed line). (b) Results for $l_2/\lambda_q = 0.25$ (red solid line) and 0.245 (green dashed line). The free-survival probability in the absence of the JQF is also shown (blue dotted).

The photon-mediated interaction between qubits can generally be divided into the effective exchange interaction and cooperative decay, as discussed in Sec. II D. From Eqs. (16) and (18), we observe that the effective exchange interaction vanishes at the optimal positions of the DQ and the JQF ($l_1 = 0$ and $l_2 = n\lambda_q/2$). Therefore, cooperative decay plays an essential role for protection of the DQ: the prohibited decay of the DQ originates in the subradiance effect [33–35]. This is understood most clearly in the case of $l_1 = l_2 = 0$. From the Hamiltonian of Eq. (2), we observe that the following two states, $|\text{sup}\rangle$ and $|\text{sub}\rangle$, respectively, correspond to the super- and subradiant states within the one-excitation subspace of the two qubits:

$$|\text{sup}\rangle = \frac{\sqrt{\gamma_1}\hat{\sigma}_1^\dagger + \sqrt{\gamma_2}\hat{\sigma}_2^\dagger}{\sqrt{\gamma_1 + \gamma_2}}|v\rangle, \quad (34)$$

$$|\text{sub}\rangle = \frac{\sqrt{\gamma_2}\hat{\sigma}_1^\dagger - \sqrt{\gamma_1}\hat{\sigma}_2^\dagger}{\sqrt{\gamma_1 + \gamma_2}}|v\rangle. \quad (35)$$

The superradiant state decays rapidly with a rate of $2(\gamma_1 + \gamma_2)$, whereas the subradiant state is an eigenstate of the Hamiltonian and does not decay. The excited state of the DQ is mostly composed of the subradiant state and contains a tiny fraction of the superradiant state:

$$\hat{\sigma}_1^\dagger|v\rangle = \frac{\sqrt{\gamma_1}|\text{sup}\rangle + \sqrt{\gamma_2}|\text{sub}\rangle}{\sqrt{\gamma_1 + \gamma_2}}. \quad (36)$$

The rapid decay of the superradiant component is observed as the initial drop of the survival probability in Fig. 2(a). The quasistationary $P_1 [= \gamma_2^2/(\gamma_1 + \gamma_2)^2]$ results from the subradiant components. These arguments are compatible with Eqs. (32) and (33) with $n = 0$.

V. MICROWAVE RESPONSE

In the previous section, we have derived the radiative decay rate of the DQ analytically and confirmed that the JQF protects the DQ from radiative decay through the control line. In this section, we numerically investigate the quantum control of a DQ with a microwave pulse applied through the waveguide. We will observe that, as long as the control pulse is sufficiently strong, we can control the DQ as if the JQF is absent. This implies that the JQF does not affect the gate time T_g of the DQ while enhancing its lifetime T_1 and thus breaks the trade-off relation of Eq. (22).

We assume that both qubits are in the ground state at the initial moment ($t = 0$) and that a classical control field $E_{\text{in}}(t)$ is applied through the waveguide for $t > 0$. The spatial waveform of the control field at $t = 0$ is $E_{\text{in}}(-r)$.

Therefore, the initial state vector is written as

$$|\phi(0)\rangle = \mathcal{N} \exp\left(\int_{-\infty}^0 dr E_{\text{in}}(-r) \tilde{b}_r^\dagger\right)|v\rangle, \quad (37)$$

where $\mathcal{N} = \exp(-\int dr |E_{\text{in}}(-r)|^2/2)$ is a normalization factor. Note that this is in a coherent state and therefore is an eigenvector of the noise operator, Eq. (13). Hereafter, we use the notation of $\langle\phi(0)|\hat{A}(t)|\phi(0)\rangle = \langle\hat{A}(t)\rangle$. From Eqs. (14) and (37), the equation of motion for $\langle\hat{\sigma}_1(t)\rangle$ is given by

$$\begin{aligned} \frac{d}{dt}\langle\hat{\sigma}_1\rangle &= (-i\omega_q - \xi_{11})\langle\hat{\sigma}_1\rangle - \xi_{12}\langle\hat{\sigma}_2\rangle + 2\xi_{12}\langle\hat{\sigma}_1^\dagger\hat{\sigma}_1\hat{\sigma}_2\rangle \\ &\quad + i(1 - 2\langle\hat{\sigma}_1^\dagger\hat{\sigma}_1\rangle)\langle\hat{N}_1(t)\rangle, \end{aligned} \quad (38)$$

where

$$\langle\hat{N}_m(t)\rangle = \sqrt{2\gamma_m} \cos(\omega_q t_m) E_{\text{in}}(t). \quad (39)$$

We numerically solve the simultaneous differential equations of the following nine quantities: $\langle\hat{\sigma}_1\rangle$, $\langle\hat{\sigma}_2\rangle$, $\langle\hat{\sigma}_1^\dagger\hat{\sigma}_1\rangle$, $\langle\hat{\sigma}_2^\dagger\hat{\sigma}_2\rangle$, $\langle\hat{\sigma}_2^\dagger\hat{\sigma}_1\rangle$, $\langle\hat{\sigma}_1\hat{\sigma}_2\rangle$, $\langle\hat{\sigma}_1^\dagger\hat{\sigma}_1\hat{\sigma}_2\rangle$, $\langle\hat{\sigma}_2^\dagger\hat{\sigma}_1\hat{\sigma}_2\rangle$, and $\langle\hat{\sigma}_1^\dagger\hat{\sigma}_2^\dagger\hat{\sigma}_1\hat{\sigma}_2\rangle$. Note that these equations are closed under the free-evolution approximations employed in Sec. II C.

A. Rabi oscillation

First, we investigate the case of continuous drive,

$$E_{\text{in}}(t) = \begin{cases} 0, & t < 0, \\ E_d e^{-i\omega_d t}, & t \geq 0, \end{cases} \quad (40)$$

and observe the Rabi oscillations of the DQ and the JQF induced by this drive field. Note that $|E_d|^2$ represents the incoming photon rate. In the numerical simulations, we assume that both the DQ and the JQF are placed at their optimal positions ($l_1 = 0$, $l_2 = \lambda_q/2$) and that a resonant drive field ($\omega_d = \omega_q$) is applied through the waveguide.

In Fig. 3, the excitation probabilities of the DQ and the JQF, $P_m(t) = \langle\hat{\sigma}_m^\dagger\hat{\sigma}_m\rangle$, are plotted for various values of the drive power. In order to emphasize the effect of the JQF on the DQ, we also plot the *free* Rabi oscillation of the DQ, $P_{1f}(t)$, assuming the absence of the JQF. $P_{1f}(t)$ is analytically given by

$$P_{1f}(t) = \frac{\Omega_1^2}{2(\Omega_1^2 + 2\gamma_1^2)} \left[1 - e^{-3\gamma_1 t/2} \left(\cos \widetilde{\Omega}_1 t + \frac{3\gamma_1}{2\widetilde{\Omega}_1} \sin \widetilde{\Omega}_1 t \right) \right], \quad (41)$$

where $\Omega_1 = \sqrt{8\gamma_1|E_d|^2}$ (Rabi frequency) and $\widetilde{\Omega}_1 = \sqrt{8\gamma_1|E_d|^2 - (\gamma_1/2)^2}$. We observe that $P_1(t)$ and $P_{1f}(t)$

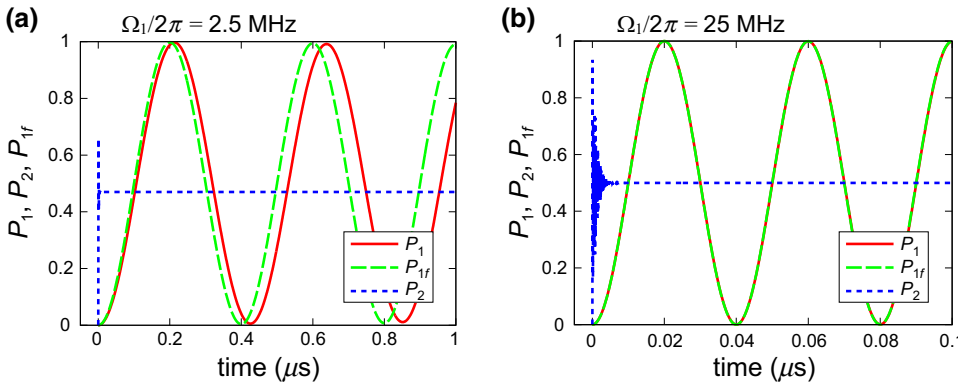


FIG. 3. The Rabi oscillations of the DQ (P_1 , red solid line) and the JQF (P_2 , blue dotted line). The free Rabi oscillation of the DQ (P_{1f} , green dashed line) in the absence of the JQF is also shown for reference. The Rabi frequency is set at $\Omega_1/2\pi = 2.5$ MHz in (a) and at 25 MHz in (b). The corresponding photon rates are $|E_d|^2/\gamma_2 = 3.91$ and 391, respectively. P_1 and P_{1f} are almost overlapping in (b).

are almost overlapping for a strong drive satisfying $\gamma_2 \ll |E_d|^2$. Thus, the Rabi oscillation of the DQ is almost unaffected by the JQF. This is explained as follows. In the right-hand side of Eq. (14), we see that the DQ is driven by two different mechanisms: the mutual interaction between the DQ and the JQF (second term) and the applied field (third term). Therefore, the condition that the Rabi oscillation of the DQ is unaffected by the JQF is $|\xi_{12}| \ll \langle \hat{N}_1(t) \rangle$, which reduces to $\gamma_2 \ll |E_d|^2$.

On the other hand, the JQF undergoes a much faster Rabi oscillation than the DQ ($\Omega_2/\Omega_1 = \sqrt{\gamma_2/\gamma_1} \approx 224$)

and relaxes to its stationary value of $\Omega_2^2/2(\Omega_2^2 + 2\gamma_2^2)$ within a relaxation time of $\gamma_2^{-1} \sim 5$ ns. For a strong field satisfying $|E_d|^2 \gg \gamma_2$, the JQF becomes saturated and the stationary state is approximately the maximally mixed state.

B. π -pulse excitation

Here, we observe the dynamics of the DQ and the JQF induced by a π pulse for the DQ. We employ a square π pulse with a length of 20 ns ($\Omega_1/2\pi = 25$ MHz). The time

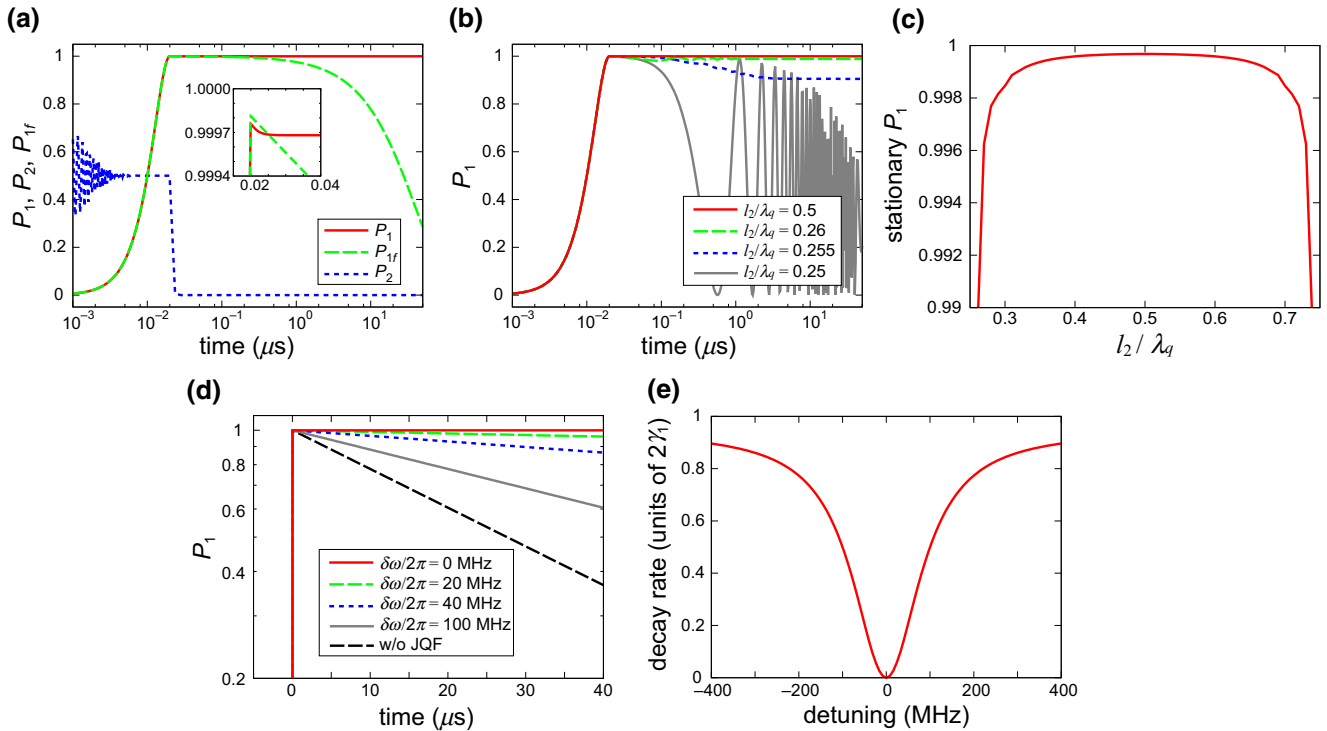
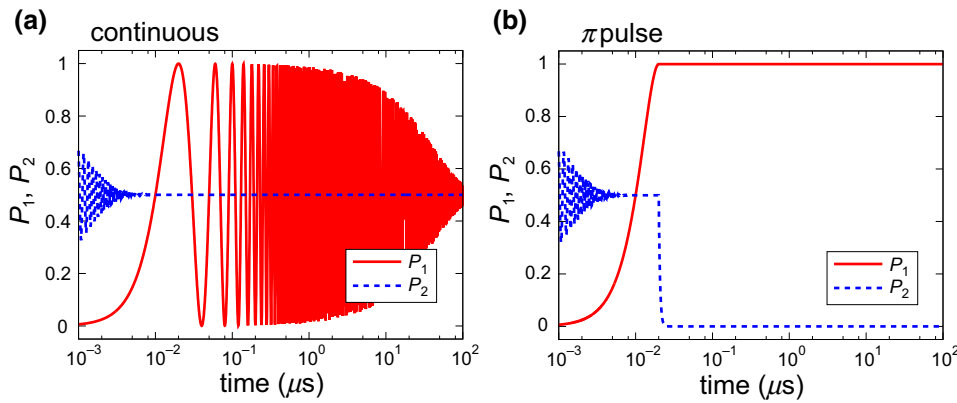


FIG. 4. The response to the π pulse. The pulse is on for $0 \leq t \leq 20$ ns. (a) The excitation probability of the DQ (P_1 , red solid line) and the JQF (P_2 , blue dotted line). The former in the absence of the JQF (P_{1f} , green dashed line) is also plotted. P_1 and P_{1f} are overlapping for $t \lesssim 0.2$ μ s. The inset shows the evolution of P_1 and P_{1f} just after the π -pulse excitation ($t \sim 0.02$ μ s). (b) $P_1(t)$ for various JQF positions l_2 . (c) The dependence of the stationary value of P_1 (measured at 10 μ s) on the JQF position l_2 . (d) $P_1(t)$ for various JQF frequencies ω_2 . The detuning $\delta\omega$ in the legend is defined by $\delta\omega = \omega_2 - \omega_1$. (e) The dependence of the radiative decay rate of the DQ on the detuning.



evolution of the excitation probabilities of the DQ (P_1) and the JQF (P_2) is plotted in Fig. 4(a). The JQF exhibits a rapid damped Rabi oscillation and relaxes to the maximally mixed state ($P_2 = 1/2$) during π -pulse irradiation. After the π pulse is switched off, the JQF quickly decays to the ground state. On the other hand, the DQ is excited by the π pulse and remains in the excited state even after the π pulse is switched off. The stationary value of P_1 is 0.99968. There are two reasons for the tiny unexcited probability of 0.00032, as follows. The principal reason is the damping of the DQ during π -pulse irradiation. As we observe later (Fig. 5), damping of the DQ is not suppressed while the control field is on. The secondary reason is the drop of P_1 after the π -pulse irradiation. Here, this value amounts to 7.94×10^{-5} [inset of Fig. 4(a)], which is larger than 4.00×10^{-5} observed in Fig. 2(a). This difference originates in imperfect initialization of the JQF: it is assumed to be completely in the ground state in Fig. 2(a), whereas it is in the maximally mixed state in Fig. 4(a).

The JQF position l_2 is varied in Fig. 4(b) and the stationary excitation probability (P_1 at $t = 10 \mu\text{s}$) is plotted as a function of l_2 in Fig. 4(c). A remarkable fact here is that the decay of the DQ is prohibited even when the JQF

is not placed exactly at its optimal position. For example, the stationary excitation probability reaches 0.9994 for $l_2/\lambda_q = 0.35$ (nonoptimal), which is comparable to 0.9997 for $l_2/\lambda_q = 0.5$ (optimal). Therefore, precise positioning of the JQF is unnecessary for protection of the DQ. This makes practical implementation of the present scheme easier.

The JQF frequency ω_2 is varied in Fig. 4(d). We observe that, in the presence of detuning, the protection of the DQ by the JQF is imperfect, resulting in the exponential decay of the DQ. In Fig. 4(e), the DQ decay rate is plotted as a function of the detuning. The functional form of this decay rate is given by Eq. (B4). The width of the dip in the decay rate is about 200 MHz, which is determined by the JQF line width γ_2 .

Continuous-wave and π -pulse excitations are compared in Fig. 5. Under continuous-wave excitation [Fig. 5(a)], the JQF is in the maximally mixed state and transmits radiation from the DQ. Therefore, while the control field is on, the control line works as a dissipation channel and damps the dynamics of the DQ. In contrast, after the π -pulse excitation [Fig. 5(b)], the JQF immediately decays to the ground state and reflects the microwave photons emitted by the

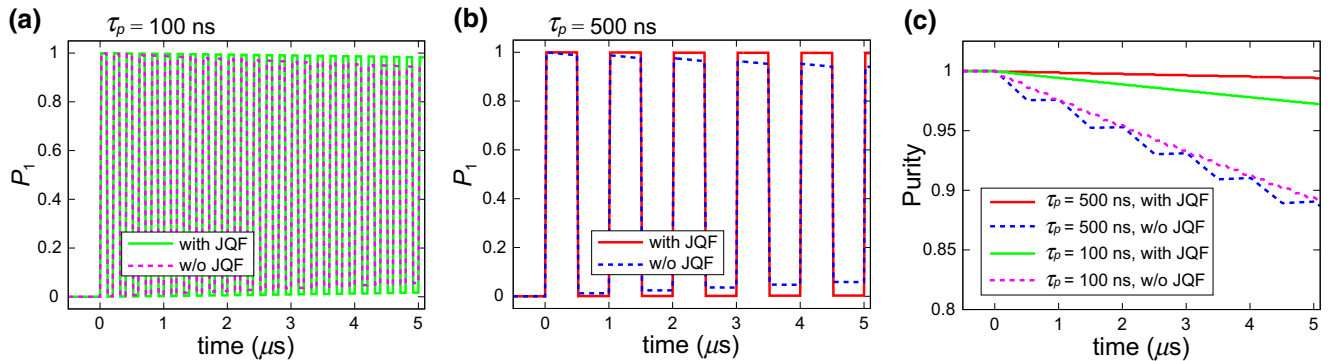


FIG. 6. The successive application of π pulses. The π -pulse duration time is 20 ns. (a) The time evolution of the excitation probability of the DQ with the pulse period $\tau_p = 100 \text{ ns}$. The green solid (magenta dotted) line shows the results with (without) the JQF. (b) The same plot as (a) for $\tau_p = 500 \text{ ns}$. The red solid (blue dotted) line shows the results with (without) the JQF. (c) The time evolution of the purity of the DQ. The upper (lower) two lines show the results with (without) the JQF.

DQ. Therefore, while the control field is off, the DQ is decoupled from the control line and stays in the excited state without being dissipated.

In Fig. 6, we show the bit flips of the DQ between the ground and excited states induced by successive π pulses. The π -pulse duration time is set at 20 ns and the pulse period τ_p is set at 100 ns (duty ratio 0.2) in Fig. 6(a) and at 500 ns (duty ratio 0.04) in Fig. 6(b). Without the JQF, the amplitude of P_1 oscillation damps with a rate around γ_1 : P_1 at $t = 5.02 \mu\text{s}$ is 0.9436 in (a) and 0.9417 in (b). The damping rate is almost insensitive to the duty ratio, since damping of the DQ always occurs, regardless of whether the control pulse is on or off. In the presence of the JQF, damping of the DQ is substantially suppressed: P_1 at $t = 5.02 \mu\text{s}$ reaches 0.9828 in (a) and 0.9968 in (b). Operation with the lower duty ratio is more advantageous, since the JQF only protects the DQ while the control pulse is off. This is also confirmed in Fig. 6(c), which plots the time evolution of the purity of the DQ, $\mathcal{P} = \langle \hat{\sigma}_1^\dagger \hat{\sigma}_1 \rangle^2 + (1 - \langle \hat{\sigma}_1^\dagger \hat{\sigma}_1 \rangle)^2 + 2|\langle \hat{\sigma}_1 \rangle|^2$.

VI. SUMMARY

For scalable quantum information processing, we should perform fast gate operations on the qubits, while keeping long coherence times of the qubits. However, there exists a trade-off between them, which cannot be resolved by a conventional Purcell filter. In this work, we propose a JQF that protects a DQ from radiative decay into the control line without losing the gate speed. In the proposed setup, a DQ is coupled to one end of a semi-infinite control line and a JQF is coupled to the same line with a distance from the DQ of the order of resonance wavelength. Owing to a subradiance effect, the JQF suppresses radiative decay of the DQ under the following conditions: (i) the DQ and the JQF are resonant, (ii) the JQF couples to the control line far more strongly than the DQ, and (iii) the DQ-JQF distance is close to integer multiples of half of the resonance wavelength. We numerically confirm that the speed of the gate operations on the DQ is unaffected by the JQF. The radiative decay of the DQ is completely suppressed by the JQF when the control field is off, whereas it is not under irradiation of the control field. Thus, the operation of the JQF is somewhat similar to that of a tunable coupler between a qubit and a control line. However, the JQF is a passive element that is free from the imposition of active control and therefore is highly suitable for integration in complicated circuits with many qubits.

ACKNOWLEDGMENTS

We acknowledge the fruitful discussions with S. Masuda, T. Shitara, and J. Gea-Banacloche. This work was supported in part by the Japan Society for the

Promotion of Science (JSPS) Grants-in-Aid for Scientific Research (KAKENHI) (Grants No. 19K03684 and No. 26220601), the Japan Science and Technology Agency (JST) Exploratory Research for Advanced Technology (ERATO) (Grant No. JPMJER1601), the University of Tokyo Advanced Leading Graduate Course for Photon Science (ALPS), and the Ministry of Education, Culture, Sports, Science, and Technology Quantum Leap Flagship Program (MEXT Q-LEAP) (Grant No. JPMXS0118068682).

APPENDIX A: VALIDATION OF FREE-EVOLUTION APPROXIMATION

In this appendix, in order to check the validity of the free-evolution approximation, we analyze the radiative decay of the DQ without the free-evolution approximation. The initial state vector [Eq. (23)] and the state vector at time t [Eq. (24)] remain unchanged in the rigorous analysis. However, without the free-evolution approximation, the equations of motion for $\alpha_1(t)$ and $\alpha_2(t)$ become delay differential equations. Instead of Eqs. (25) and (26), they are given by

$$\begin{aligned} \frac{d}{dt}\alpha_1(t) &= \left(-i\omega_q - \frac{\gamma_1}{2}\right)\alpha_1(t) - \frac{\gamma_1}{2}\alpha_1(t-2l_1) \\ &\quad - \frac{\sqrt{\gamma_1\gamma_2}}{2}[\alpha_2(t-l_1-l_2) + \alpha_2(t+l_1-l_2)], \end{aligned} \quad (\text{A1})$$

$$\begin{aligned} \frac{d}{dt}\alpha_2(t) &= \left(-i\omega_q - \frac{\gamma_2}{2}\right)\alpha_2(t) - \frac{\gamma_2}{2}\alpha_2(t-2l_2) \\ &\quad - \frac{\sqrt{\gamma_1\gamma_2}}{2}[\alpha_1(t-l_1-l_2) + \alpha_1(t+l_1-l_2)], \end{aligned} \quad (\text{A2})$$

with the initial conditions of $\alpha_1(0) = 1$ and $\alpha_2(0) = 0$. Note that $\alpha_{1,2}(t) = 0$ for $t < 0$. When the JQF is absent ($\gamma_2 = 0$), this setup corresponds to an atom in front of a mirror [28,36,37].

In Fig. 7, fixing $l_1(=0)$ and varying l_2 , we compare the rigorous and approximate survival probabilities $P_1(t) = |\alpha_1(t)|^2$. The upper three lines in Fig. 7(a) represent the rigorous ones for $l_2/\lambda_q = 0.5$ and 2.5 and the approximate one. Note that the free-evolution approximation yields the same $P_1(t)$ for $l_2/\lambda_q = 0.5$ and 2.5. As expected, the agreement between the rigorous and approximate results becomes better for a shorter round-trip time $2l_2$. The deviation between the rigorous and approximate $P_1(t)$ is negligibly small for $l_2/\lambda_q = 0.5$ (2.6×10^{-6} in the stationary state), indicating the validity of the approximation. The lower three lines in Figs. 7(a) and 7(b) show the results for the nonoptimal filter position. The deviation between

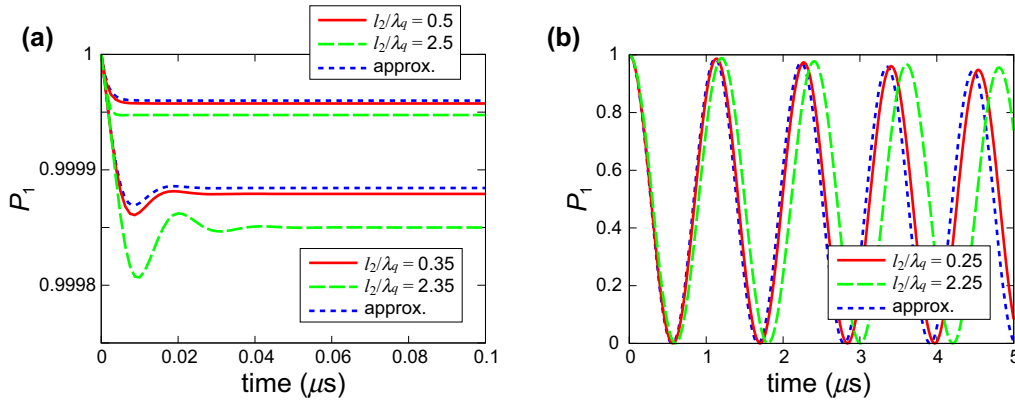


FIG. 7. A comparison of the rigorous survival probability and the approximate ones based on the free-evolution approximation.

the rigorous and approximate results is larger in comparison with the optimal cases, but the approximation is fairly good for $l_2 \lesssim \lambda_q$.

APPENDIX B: EFFECT OF INTRINSIC LOSS AND DETUNING

Here, we derive the decay rate of the DQ in the presence of the intrinsic loss of the DQ and the JQF and the detuning between them. We denote the intrinsic decay rates of the DQ and the JQF by γ_{11} and γ_{12} , respectively. Then, Eqs. (25) and (26) are modified as follows:

$$\frac{d\alpha_1}{dt} = -(i\omega_1 + \xi_{11} + \gamma_{11}/2)\alpha_1 - \xi_{12}\alpha_2, \quad (\text{B1})$$

$$\frac{d\alpha_2}{dt} = -\xi_{21}\alpha_1 - (i\omega_2 + \xi_{22} + \gamma_{12}/2)\alpha_2. \quad (\text{B2})$$

Switching to the frame rotating at ω_1 and solving Eq. (B2) adiabatically, the complex frequency of the DQ is given by

$$\tilde{\omega}_1' = \omega_q + i \left(\frac{\xi_{12}\xi_{21}}{\xi_{22} + \gamma_{12}/2 + i\delta\omega} - \xi_{11} - \frac{\gamma_{11}}{2} \right), \quad (\text{B3})$$

where $\delta\omega = \omega_2 - \omega_1$ is the detuning between the DQ and the JQF. The decay rate of the DQ is determined by $\gamma_{\text{DQ}} = -2\text{Im}(\tilde{\omega}_1')$. For the optimal case of $l_1 = 0$ and $l_2 = n\lambda_q/2$ ($n = 0, 1, \dots$), γ_{DQ} reduces to the following form:

$$\gamma_{\text{DQ}} = \gamma_{11} + 2\gamma_1 \left[1 - \frac{\gamma_2(\gamma_2 + \gamma_{12}/2)}{(\gamma_2 + \gamma_{12}/2)^2 + (\delta\omega)^2} \right]. \quad (\text{B4})$$

The first term represents the intrinsic decay rate of the DQ, which is unaffected by the JQF, as expected. The second term represents the radiative decay rate of the DQ, which is suppressed by the JQF. In the absence of detuning and in the $\gamma_2 \gg \gamma_{12}$ limit, the radiative decay rate of the DQ is approximately given by $\gamma_1 \times (\gamma_{12}/\gamma_2)$. This implies that,

even when the JQF has intrinsic loss, we can substantially suppress the radiative decay of the DQ by making the radiative decay of the JQF dominant. Equation (B4) agrees with the Lorentzian dip observed in Fig. 4(d).

- [1] R. Barends *et al.*, Superconducting quantum circuits at the surface code threshold for fault tolerance, *Nature* **508**, 500 (2014).
- [2] J. Kelly *et al.*, State preservation by repetitive error detection in a superconducting quantum circuit, *Nature* **519**, 66 (2015).
- [3] M. Reagor *et al.*, Demonstration of universal parametric entangling gates on a multi-qubit lattice, *Sci. Adv.* **4**, eaao3603 (2018).
- [4] C. Song, K. Xu, H. Li, Y. Zhang, X. Zhang, W. Liu, Q. Guo, Z. Wang, W. Ren, J. Hao, H. Feng, H. Fan, D. Zheng, D. Wang, H. Wang, and S. Zhu, Observation of multi-component atomic Schrödinger cat states of up to 20 qubits, *Science* **365**, 574 (2019).
- [5] K. X. Wei, I. Lauer, S. Srinivasan, N. Sundaresan, D. T. McClure, D. Toyli, D. C. McKay, J. M. Gambetta, and S. Sheldon, Verifying multipartite entangled GHz states via multiple quantum coherences, arXiv:1905.05720.
- [6] Y. Ye *et al.*, Propagation and Localization of Collective Excitations on a 24-Qubit Superconducting Processor, *Phys. Rev. Lett.* **123**, 050502 (2019).
- [7] A. Blais, R.-S. Huang, A. Wallraff, S. M. Girvin, and R. J. Schoelkopf, Cavity quantum electrodynamics for superconducting electrical circuits: An architecture for quantum computation, *Phys. Rev. A* **69**, 062320 (2004).
- [8] R. Vijay, D. H. Slichter, and I. Siddiqi, Observation of Quantum Jumps in a Superconducting Artificial Atom, *Phys. Rev. Lett.* **106**, 110502 (2011).
- [9] P. Krantz, M. Kjaergaard, F. Yan, T. P. Orlando, S. Gustavsson, and W. D. Oliver, A quantum engineer's guide to superconducting qubits, *Appl. Phys. Rev.* **6**, 021318 (2019).
- [10] N. Bloembergen, E. M. Purcell, and R. V. Pound, Relaxation effects in nuclear magnetic resonance absorption, *Phys. Rev.* **73**, 679 (1948).
- [11] M. D. Reed, B. R. Johnson, A. A. Houck, L. DiCarlo, J. M. Chow, D. I. Schuster, L. Frunzio, and R. J. Schoelkopf, Fast reset and suppressing spontaneous emission of a superconducting qubit, *Appl. Phys. Lett.* **96**, 203110 (2010).

- [12] E. A. Sete, J. M. Martinis, and A. N. Korotkov, Quantum theory of a bandpass Purcell filter for qubit readout, *Phys. Rev. A* **92**, 012325 (2015).
- [13] D. Sank, E. Jeffrey, J. Y. Mutus, T. C. White, J. Kelly, R. Barends, Y. Chen, Z. Chen, B. Chiaro, A. Dunsworth, A. Megrant, P. J. J. O’Malley, C. Neill, P. Roushan, A. Vainsencher, J. Wenner, A. N. Cleland, and J. M. Martinis, Fast Accurate State Measurement with Superconducting Qubits, *Phys. Rev. Lett.* **112**, 190504 (2014).
- [14] T. Walter, P. Kurpiers, S. Gasparinetti, P. Magnard, A. Potocnik, Y. Salathe, M. Pechal, M. Mondal, M. Oppliger, C. Eichler, and A. Wallraff, Rapid High-Fidelity Single-Shot Dispersive Readout of Superconducting Qubits, *Phys. Rev. Appl.* **7**, 054020 (2017).
- [15] J.-T. Shen and S. Fan, Coherent Single Photon Transport in a One-Dimensional Waveguide Coupled with Superconducting Quantum Bits, *Phys. Rev. Lett.* **95**, 213001 (2005).
- [16] J.-T. Shen and S. Fan, Coherent photon transport from spontaneous emission in one-dimensional waveguides, *Opt. Lett.* **30**, 2001 (2005).
- [17] O. Astafiev, A. M. Zagoskin, A. A. Abdumalikov, Jr., Yu. A. Pashkin, T. Yamamoto, K. Inomata, Y. Nakamura, and J. S. Tsai, Resonance fluorescence of a single artificial atom, *Science* **327**, 840 (2010).
- [18] K. Koshino, H. Terai, K. Inomata, T. Yamamoto, W. Qiu, Z. Wang, and Y. Nakamura, Observation of Three-State Dressed States in Circuit Quantum Electrodynamics, *Phys. Rev. Lett.* **110**, 263601 (2013).
- [19] X. Gu, A. F. Kockum, A. Miranowicz, Y. Liu, and F. Nori, Microwave photonics with superconducting quantum circuits, *Phys. Rep.* **718–719**, 1 (2017).
- [20] E. A. Sete, A. Galiautdinov, E. Mlinar, J. M. Martinis, and A. N. Korotkov, Catch-Disperse-Release Readout for Superconducting Qubits, *Phys. Rev. Lett.* **110**, 210501 (2013).
- [21] C. Bockstiegel, Y. Wang, M. R. Vissers, L. F. Wei, S. Chaudhuri, J. Hubmayr, and J. Gao, A tunable coupler for superconducting microwave resonators using a nonlinear kinetic inductance transmission line, *Appl. Phys. Lett.* **108**, 222604 (2016).
- [22] P. Forn-Diaz, C. W. Warren, C. W. S. Chang, A. M. Vadiraj, and C. M. Wilson, On-Demand Microwave Generator of Shaped Single Photons, *Phys. Rev. Appl.* **8**, 054015 (2017).
- [23] This introduces the modes with negative energies. However, such modes are highly detuned from the qubits and have little effect on the dynamics.
- [24] J. Gea-Banacloche, Space-time descriptions of quantum fields interacting with optical cavities, *Phys. Rev. A* **87**, 023832 (2013).
- [25] C. W. Gardiner and P. Zoller, *Quantum Noise: A Handbook of Markovian and Non-Markovian Quantum Stochastic Methods with Applications to Quantum Optics* (Springer, Berlin, 2004), 3rd ed.
- [26] D. F. Walls and G. J. Milburn, *Quantum Optics* (Springer, Berlin, 2007), 2nd ed.
- [27] J. R. Johansson, L. G. Mourokh, A. Yu. Smirnov, and F. Nori, Enhancing the conductance of a two-electron nanomechanical oscillator, *Phys. Rev. B* **77**, 035428 (2008).
- [28] K. Koshino and Y. Nakamura, Control of the radiative level shift and linewidth of a superconducting artificial atom through a variable boundary condition, *New J. Phys.* **14**, 043005 (2012).
- [29] D. E. Chang, L. Jiang, A. V. Gorshkov, and H. J. Kimble, Cavity QED with atomic mirrors, *New J. Phys.* **14**, 063003 (2012).
- [30] K. Lalumiere, B. C. Sanders, A. F. van Loo, A. Fedorov, A. Wallraff, and A. Blais, Input-output theory for waveguide QED with an ensemble of inhomogeneous atoms, *Phys. Rev. A* **88**, 043806 (2013).
- [31] A. F. van Loo, A. Fedorov, K. Lalumiere, B. C. Sanders, A. Blais, and A. Wallraff, Photon-mediated interactions between distant artificial atoms, *Science* **342**, 1494 (2013).
- [32] W. Konyk and J. Gea-Banacloche, One-and two-photon scattering by two atoms in a waveguide, *Phys. Rev. A* **96**, 063826 (2017).
- [33] A. Goban, C.-L. Hung, J. D. Hood, S.-P. Yu, J. A. Muniz, O. Painter, and H. J. Kimble, Superradiance for Atoms Trapped along a Photonic Crystal Waveguide, *Phys. Rev. Lett.* **115**, 063601 (2015).
- [34] L. Ostermann, C. Meignant, C. Genes, and H. Ritsch, Super- and subradiance of clock atoms in multimode optical waveguides, *New J. Phys.* **21**, 025004 (2019).
- [35] A. Albrecht, L. Henriet, A. Asenjo-Garcia, P. B. Dieterle, O. Painter, and D. E. Chang, Subradiant states of quantum bits coupled to a one-dimensional waveguide, *New J. Phys.* **21**, 025003 (2019).
- [36] I. C. Hoi, A. F. Kockum, L. Tornberg, A. Pourkabirian, G. Johansson, P. Delsing, and C. M. Wilson, Probing the quantum vacuum with an artificial atom in front of a mirror, *Nat. Phys.* **11**, 1045 (2015).
- [37] E. Wiegand, B. Rousseaux, and G. Johansson, A semiclassical analysis of dark state transient dynamics in waveguide circuit QED, arXiv:1909.05210.